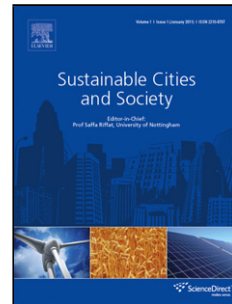


Journal Pre-proof

An experimental and numerical study on a multi-robot source localization method independent of airflow information in dynamic indoor environments

Qilin Feng, Hao Cai, Yibin Yang, Jiheng Xu, Mingrui Jiang, Fei Li,
Xianting Li, Chenchu Yan



PII: S2210-6707(19)30716-4

DOI: <https://doi.org/10.1016/j.scs.2019.101897>

Reference: SCS 101897

To appear in: *Sustainable Cities and Society*

Received Date: 16 March 2019

Revised Date: 30 July 2019

Accepted Date: 14 October 2019

Please cite this article as: Feng Q, Cai H, Yang Y, Xu J, Jiang M, Li F, Li X, Yan C, An experimental and numerical study on a multi-robot source localization method independent of airflow information in dynamic indoor environments, *Sustainable Cities and Society* (2019), doi: <https://doi.org/10.1016/j.scs.2019.101897>

This is a PDF file of an article that has undergone enhancements after acceptance, such as the addition of a cover page and metadata, and formatting for readability, but it is not yet the definitive version of record. This version will undergo additional copyediting, typesetting and review before it is published in its final form, but we are providing this version to give early visibility of the article. Please note that, during the production process, errors may be discovered which could affect the content, and all legal disclaimers that apply to the journal pertain.

© 2019 Published by Elsevier.

An experimental and numerical study on a multi-robot source localization method independent of airflow information in dynamic indoor environments

Qilin Feng², Hao Cai^{1*}, Yibin Yang³, Jiheng Xu³, Mingrui Jiang¹, Fei Li¹, Xianting Li⁴,
Chenchu Yan¹

¹ Department of HVAC, College of Urban Construction, Nanjing Tech University,
Nanjing, 210009, P.R. China

² Research Institute for National Defense Engineering of Academy of Military Science
PLA China, Beijing, 100850, P.R. China

³ College of National Defense Engineering, Army Engineering University, Nanjing,
210007, P.R. China

⁴ Department of Building Science, Tsinghua University, Beijing, 100084, P.R. China.

* Corresponding author: Hao Cai

Tel: +86-25-83239964;

E-mail: caihao@njtech.edu.cn

Highlights:

- A multi-robot source localization method independent of airflow information was presented for dynamic indoor environment.
- The method was experimentally validated in a typical dynamic indoor environment.
- The feasibility of using numerical simulations was validated.
- The method was compared with two other PSO-based source localization methods (SPSO and WUII) by numerical experiments
- The method has a higher success rate than that of the SPSO and WUII methods in mixing ventilation and natural ventilation cases.

Abstract: To locate contaminant sources in dynamic indoor environments, this study presents an improved particle swarm optimization (IPSO) method independent of airflow information and validates the method by combining robot experiments with numerical simulations. The experimental study was first conducted by using three mobile robots to locate an ethanol source in a typical dynamic indoor environment with a fan swinging periodically from left to right. A total of 12 out of 15 experiments were successful, with a success rate of 80%, indicating that the method has a high success rate and strong robustness. Next, the experimental environment was further simulated by CFD, and numerical experiments were conducted. The results show that

the success rate and the average number of steps from numerical experiments were consistent with those from robot experiments, indicating the feasibility of using numerical simulations. Finally, the IPSO method was numerically validated and compared with a standard PSO (SPSO) method and a modified PSO method with wind utilization II (WUII) in mixing ventilation (MV) and natural ventilation (NV) cases. With a similar average number of steps, the IPSO method achieved a higher success rate than the comparison methods, indicating the superiority of the IPSO method.

Keywords: dynamic airflow; indoor environment; source localization; multi-robot olfaction; experimental and numerical validation

1. Introduction

In modern society, people spend up to 90% of their time indoors [1–3], and therefore, indoor air pollution is closely related to people's health. In addition, indoor environmental safety is being threatened in many ways, such as outbreaks of SARS epidemics [4], leakages of toxic, flammable and explosive gases [5], and biological, chemical and radiological terrorist attacks [6]. How to effectively control indoor airborne pollutants or dangerous substances has become a critical issue worldwide [7, 8]. Common measures for controlling indoor airborne pollutants or hazardous substances include source control, ventilation, purification, and evacuation [9]. Among these measures, source control is the most effective and fundamental measure, and a prerequisite for the implementation of source control is the rapid and accurate

localization of the source [10, 11], which is of great significance for ensuring indoor air quality and environmental safety.

The difficulty of indoor source localization greatly depends on airflow characteristics. According to the airflow characteristics, indoor airflows can be roughly classified into two types: steady-state airflow and dynamic airflow. Dynamic airflows widely exist in natural ventilation environments where the air velocity or direction changes randomly [12]. Dynamic airflows also exist in mechanical ventilation environments when the supply air velocity or direction changes periodically or heat sources, movement, vehicles, or equipment disturb the indoor airflow. Therefore, source localization in dynamic indoor environments has important theoretical and practical significance. However, for source localization in indoor environments, most previous studies have developed methods based on steady-state airflow because considering dynamic airflows in source localization can be challenging [13].

The available methods for source localization can be generally categorized into two types: stationary sensor network methods and robot active olfaction methods [14]. Stationary sensor network methods use forward or backward models to infer the source location from sensor readings and require the installation of one or more sensors in the indoor space in advance. Most of the available studies on stationary sensor network methods have focused on steady-state indoor environments [5, 10, 15–24] (detailed reviews are provided in [6, 14]), and research on locating sources in dynamic indoor environments has rarely been reported. Wang et al. [13] proposed an

adjoint probability-based method for identifying the contaminant source location in a dynamic indoor environment. The method was validated by computational fluid dynamics (CFD) simulations and assumed that the simulated airflow data were consistent with those obtained in real-world conditions. However, most real-time dynamic airflows are difficult to accurately simulate with CFD models due to the uncertainty and complexity of dynamic airflows; such difficulty poses a great challenge to stationary sensor network methods.

Robot active olfaction methods were originally inspired by the behaviors of foraging, mate finding and predator evasion of some animals in nature [25–27]. This type of method normally uses mobile robots equipped with gas or airflow sensors to initiatively track and locate release sources and divides the process into three phases [28]: plume finding (contacting the gas), plume tracking (approaching the source), and source declaration (confirming the source). Compared with stationary sensor network methods, robot active olfaction methods do not require environmental sensor installation in advance or numerical simulations of airflow transportation and contaminant dispersion; therefore, robot active olfaction methods are promising for unknown and dynamic indoor environments.

To date, most available active olfaction methods have been tested in steady-state airflow environments [29–35], and only a few studies in recent years have reported the localization of sources in dynamic airflow environments. Compared to steady-state indoor environments, source localization in dynamic indoor environments is more difficult. First, in dynamic indoor environments, it is difficult to apply the

airflow speed and direction in the source localization method. The airflow speed and direction in these environments cannot be accurately detected by sensors in real time and are not easy to obtain by numerical simulations. Second, in dynamic indoor environments, more local extremum areas (where the concentration is higher than that in the surrounding area) will form, and the locations of these local extremum areas will also vary over time, which greatly increases the difficulty of continuously tracking the plume.

In recent years, some pioneers have attempted to locate sources in indoor dynamic environments and have proposed several multi-robot active olfaction methods, such as the adapted ant colony optimization method [36, 37], the particle swarm optimization (PSO) method [38, 39], and the modified PSO method [40, 41]. However, most of these methods were validated by numerical experiments and used airflow speed and direction to help robots avoid being trapped in local extremum areas. Although the use of anemometers can improve the performance of source localization, the use of anemometers in practice will also limit the application scope of multi-robot active olfaction methods. The reason is that anemometers that are currently available on the market, especially 3D anemometers, are usually bulky and therefore not suitable for use in some narrow or congested environments, nor for robot platforms with limited load capacity, such as nano aerial vehicles (NAVs) [42].

To overcome the difficulties caused by indoor dynamic airflow environments, this paper proposes a multi-robot active olfaction method (IPSO) independent of airflow information. The method uses an improved PSO algorithm to track the plume and

integrates the maximum concentration method and the divergence search strategy to escape from local extremum areas. The effectiveness of the method was validated by combining robot experiments with numerical simulations, and the performance of the proposed method was further compared with that of a standard PSO method (SPSO) and a modified PSO method with wind utilization II (WUII) [38].

The main contributions of this study are as follows:

- (1) A multi-robot active olfaction method independent of airflow information was developed for source localization in dynamic indoor environments. This method integrates the improved PSO algorithm presented in this study with our previously developed source declaration algorithm and the divergence search strategy to improve the success rate and efficiency of source localization.
- (2) The proposed method successfully located the contaminant source in a real dynamic mechanical ventilation environment created by using a fan that periodically swung from left to right.
- (3) The effectiveness of the proposed method was further numerically validated by comparison with the SPSO and WUII methods in indoor environments with mixing ventilation and natural ventilation systems.

2. An improved multi-robot source localization method independent of airflow information

2.1 Basic principles

The PSO algorithm has been widely used to locate sources and in other fields due

to its fast convergence, high-efficiency cooperation and simple implementation features. Nevertheless, this algorithm easily causes robots to become trapped in a local optimum rather than a contaminant source [38]. When robots are trapped in a local optimum, their search scope is limited to the local optimum area, and diversity is lost, which leads to the robots finding few, if any, additional optimum locations. To avoid trapping in a local optimum, this paper introduces extremum disturbance factors into the standard PSO algorithm and develops an improved PSO algorithm to track the plume without airflow information. The improved PSO algorithm uses extremum disturbance factors to maintain the diversity of the robots and enlarge their search scope. The greater the search ability the robots have, the harder it is for the robots to converge to local optima. Moreover, when the robots converge to a local optimum, extremum disturbance factors can still allow the robots to search a larger area and help them escape the local optimum area.

In our previous study [34], we introduced the basic principles of the standard PSO algorithm for tracking a plume in detail. For the sake of brevity, this study only describes the key characteristics of this algorithm and focuses on the difference between the standard PSO algorithm and the improved PSO algorithm. In the standard PSO algorithm, the fitness of the i -th robot R_i ($i = 1, 2, \dots, N$) at time step t is denoted by $c_i(t)$, namely, the contaminant concentration detected by R_i . The velocity vector and location of R_i from time step t to $t+1$ are updated as:

$$\mathbf{V}_i(t+1) = w \times \mathbf{V}_i(t) + l_1 \times r_1 \times \mathbf{P}_i^*(t) - \mathbf{P}_i(t) + l_2 \times r_2 \times \mathbf{P}_g^*(t) - \mathbf{P}_i(t) \quad (1)$$

$$\mathbf{P}_i(t+1) = \mathbf{P}_i(t) + V_i \cdot t + 1 \quad (2)$$

where $\mathbf{P}_i \cdot t$ and $V_i \cdot t$ are the location and velocity vector of R_i at time step t , respectively; w is a dimensionless inertia weight that controls how much the current velocity of a robot contributes to its velocity in the next time step; and l_1 and l_2 are dimensionless learning factors that reflect the experiences learned by a robot based on its movement and those learned by the robot swarm, respectively. According to previous experience [38], w , l_1 and l_2 were set to 1.0, 2.0 and 2.0, respectively (for a detailed explanation, refer to [34]). $\mathbf{P}_i^* \cdot t$ and $\mathbf{P}_g^* \cdot t$ are the best local location of R_i , where the concentration of R_i achieves its maximum value $c_i^* \cdot t$, and the best global location of the robot swarm, where the concentration of the robot swarm achieves its maximum value $c^* \cdot t = \max c_1^* \cdot t, c_2^* \cdot t, \dots, c_N^* \cdot t$, respectively.

In the improved PSO algorithm, the velocity vector of R_i is updated with extremum disturbance factors as:

$$V_i \cdot t + 1 = w \times V_i \cdot t + l_1 \times r_1 \times \mathbf{P}_i^{**} \cdot t - \mathbf{P}_i \cdot t + l_2 \times r_2 \times \mathbf{P}_g^{**} \cdot t - \mathbf{P}_i \cdot t \quad (4)$$

$$\mathbf{P}_i^{**} \cdot t = \mathbf{P}_i^* \cdot t + V_{\max} \times l_3 \times \mathbf{P}_i^r \quad (5)$$

$$\mathbf{P}_g^{**} \cdot t = \mathbf{P}_g^* \cdot t + V_{\max} \times l_4 \times \mathbf{P}_g^r \quad (6)$$

where V_{\max} is the maximum magnitude of the velocity vector of each robot, namely, the maximum step length of each robot. \mathbf{P}_i^r and \mathbf{P}_g^r are two disturbance vectors uniformly distributed in the range of [-1, 1]. With variations in \mathbf{P}_i^r and \mathbf{P}_g^r , the best local location $\mathbf{P}_i^* \cdot t$ and the best global location $\mathbf{P}_g^* \cdot t$ are disturbed differently, and the magnitude and direction of the velocity vector of each robot also change, which can enhance the search ability of the robot swarm and help the robots explore

more optimum locations. l_3 and l_4 are dimensionless parameters that reflect the disturbance magnitudes of two disturbance vectors on $\mathbf{P}_i^* t$ and $\mathbf{P}_g^* t$, respectively. Greater values of l_3 and l_4 can enlarge the search scope of the robot swarm but allow each robot to move farther from the optimum location. l_3 and l_4 can be reasonably determined from a certain number of robot experiments or numerical experiments for specific cases. In this study, l_3 and l_4 were set to 0.5 and 0.5, respectively.

To quickly find the contaminant plume, the divergence search strategy [11] was used in the plume finding stage. According to the divergence search strategy, all the robots depart from the starting positions and move toward different directions at the same speed until the plume is found, which is signified when a robot detects a contaminant concentration higher than the preset threshold c_{\min} . In practical applications, c_{\min} can usually be set to the detection threshold of the specific sensor carried by the robot [25].

During the plume tracking process, if the variation in the best global location $\mathbf{P}_g^* t$ within a time ΔT is not greater than the maximum step length of the robots, namely, $\max \left| \mathbf{P}_g^* t - j - \mathbf{P}_g^* t - k \right| \leq V_{\max}$, the robots believe that they have found an optimum and cannot easily find a higher concentration by using the improved PSO algorithm. At this time, the robots switch to the source declaration stage and determine whether the optimum location is in the vicinity of the source or just in a local extremum area away from the source according to the maximum concentration

method. If the concentration $c^* t$ detected at the best global location is not less than the preset concentration threshold c_{\max} for source declaration, they will determine that the best global location is in the vicinity of the source and terminate the source localization process. Otherwise, the robots will determine that the best global location is in a local extremum area, and they will use the divergence search strategy to find higher concentration values and escape from this area.

2.2 Framework and procedure

Our method consists of four main processes, as shown in Fig. 1. First, the robots depart from the starting positions using the divergence search strategy to cover as much area as possible. Second, when the concentration detected by one robot is higher than c_{\min} , all the robots switch to track the plume using the improved PSO algorithm. Third, during the plume tracking process, when the robots find a local extremum area, they subsequently confirm the source using the maximum concentration method. Fourth, if the concentration $c^* t$ is lower than c_{\max} , the robots continue to diverge using the divergence search strategy to escape from the local extremum area and rediscover the source. If the concentration $c^* t$ is not less than c_{\max} , the robots terminate the source localization procedure.

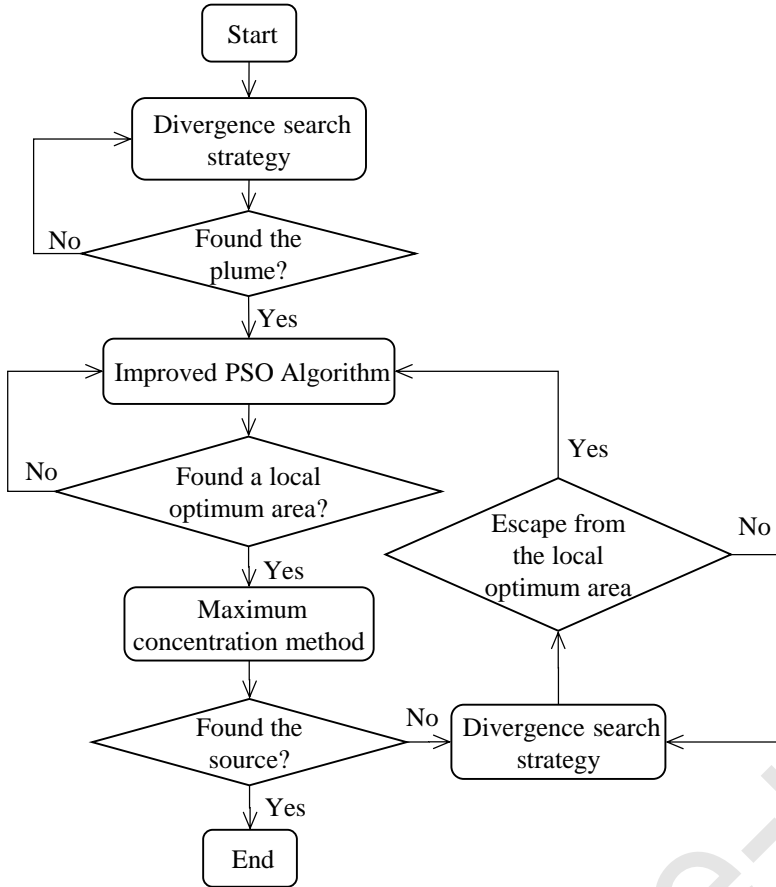


Fig. 1. Procedures of the improved multi-robot source localization method without using airflow information

3. Experimental and numerical case study

3.1 Research framework

Experimental research has the advantage of high credibility, but it also has the drawbacks of a long research period and high cost. In contrast, numerical research has the advantages of a short research period and low cost. In this study, we combined robot experiments with numerical simulations to validate the effectiveness of the proposed method (Fig. 2). As shown in Fig. 2, the validation was generally divided into three parts. First, the method was tested by robot experiments in a real indoor

environment. Second, numerical simulations of the robot experiments were conducted, and the simulated results were further compared with experimental results. The comparison showed that the results of the numerical experiments agreed well with those of the robot experiments, which verified the feasibility of the numerical validation of the presented source localization method. Finally, the numerical simulations were used to further validate the adaptability of the proposed method in indoor dynamic environments by using two typical cases (mechanical ventilation case and natural ventilation case).

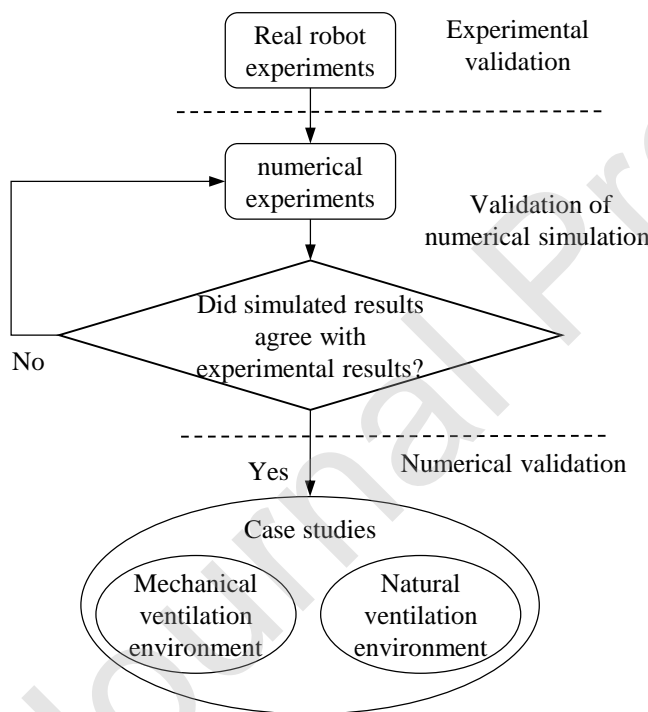


Fig. 2. Framework of the experimental and numerical validations

3.2 Setup of the robot experiments

The robot experiments were conducted in a laboratory with a length of 6.6 m and

a width of 4.9 m (Fig. 3). The area on the west side of the laboratory ($5.3\text{ m} \times 4.9\text{ m}$) was used for source localization experiments, and the movements of robots were limited within this area. In other areas, there were a desk, a chair, a cabinet air conditioner, a fan and a source release device. During each experiment, the southwestern door was kept open, and the fan periodically swung from left to right to create a typical dynamic mechanical ventilation environment. In addition, during each experiment, to avoid interference, all the windows and the southeast door were closed, and the cabinet air conditioner was turned off.

Ethanol vapor is widely used as a tracer gas in source localization research because it is minimally toxic, volatile and easily detectable [43]. During each experiment, a water bath ($60\text{ }^{\circ}\text{C}$) was used to heat liquid ethanol in a flask to control the evaporation rate at 12.5 mg/s , and an air pump was used to transport the ethanol vapor through a rubber pipe to a specific release location (Fig. 3(b)). In this study, the source was located on the downwind side of the fan ($X=4.2\text{ m}$, $Y=3.5\text{ m}$). The height of the source was set to 0.55 m , which is exactly the height of the center of the fan blade. The main reasons for choosing this source location include the following: First, this location in the downwind zone is greatly affected by the periodic variations in air supply direction and can reflect the characteristics of dynamic airflow; and second, when the source is located in the downwind zone, the spread of contaminants or hazardous substances is usually faster. Therefore, this location is a more noteworthy location.

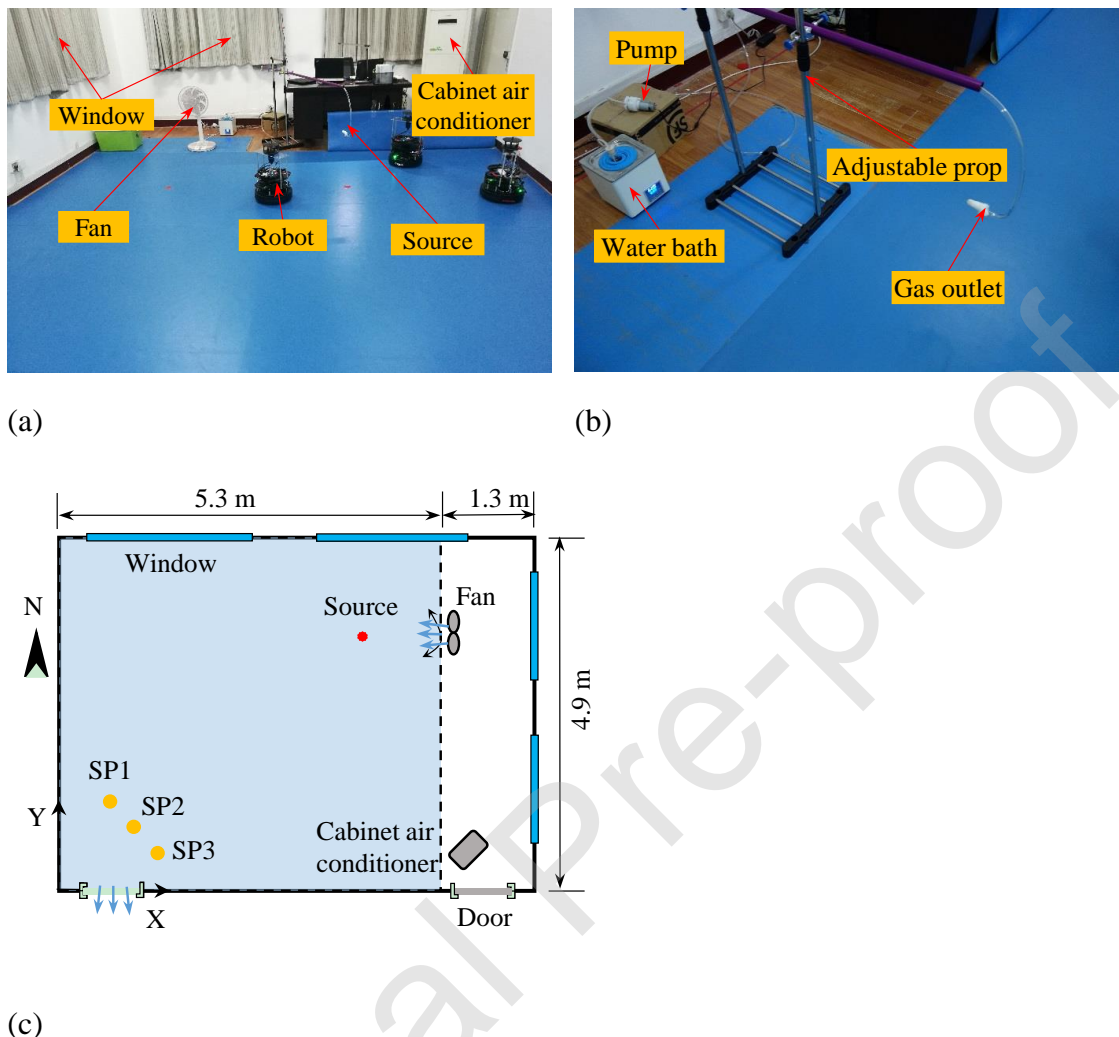


Fig. 3. Experimental site: (a) Site photo; (b) Source release device; (c) Schematic of the experimental area (SP1–SP3: starting positions of the robots)

Table 1. Starting positions of the robots

Number	Coordinate (m)	
	X	Y
SP1	0.70	1.40

SP2	1.05	1.05
SP3	1.40	0.70

To test the source localization method, we developed a multi-robot source localization system using three TurtleBot2 (Willow Garage) mobile robots. The TurtleBot2 robot not only has the ability to autonomously navigate and move (autonomous obstacle avoidance and path planning according to target position) but also has high positioning accuracy (line error: ± 5 cm, angle error: $\pm 5^\circ$). Each robot carried an embedded single-board computer (NVIDIA Jetson TK1), a laser ranging radar (RPlidar A1) and a gas sensor (Fig. 4). The single-board computer controlled the robots through the robotics middleware Robot Operating System (ROS). The laser ranging radar (RPlidar A1) was combined with the robot's own odometer for navigation and location, and the gas sensor (MICS 5524: accuracy of $\pm 3\%$ @130 ppm and response time of 2 s) was used to detect the ethanol concentration. MICS 5524 is a kind of metal oxide (MOX) sensor. When this sensor contacts a detectable gas, the conductivity or resistance will change. A simple electrical circuit can convert the change in resistance to an output signal that corresponds to the gas concentration [37]. According to the circuit principle, the actual gas concentration value can be converted according to the output voltage of the gas sensor.

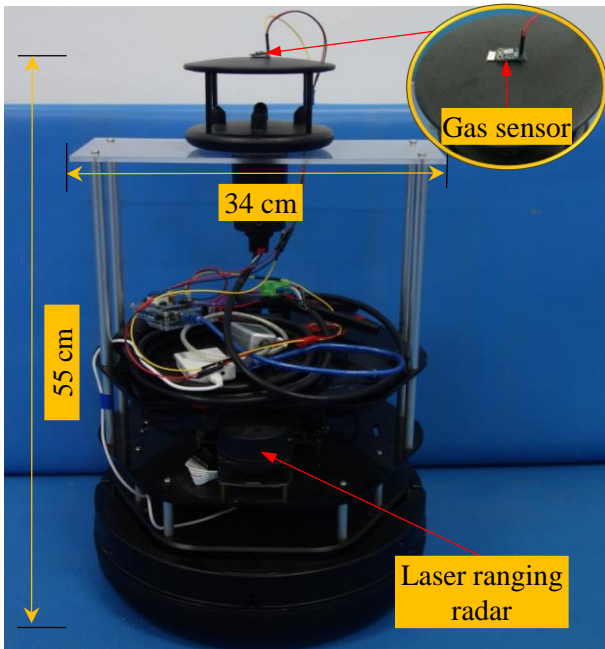


Fig. 4. Configuration of the TurtleBot2 mobile robot

Before each experiment began, the windows and doors were opened to remove the remaining ethanol vapor until the indoor ethanol concentration was less than 5 ppm. Then, except for the southwestern door, the windows and other doors were closed, the fan and the air pump were turned on, and the robots were placed in standby at their starting positions (Fig. 3(c) and Table 1). After ethanol vapor had been released for approximately 60 s, the robots started to move according to the source localization method.

During each experiment, the robots adopted the “move-stop-move” strategy [37]; that is, after each robot moved forward one step, it stayed for a certain time to collect ethanol concentrations and then continued to move. Each robot moved forward one step for approximately 10 s and then stopped and collected concentrations for 5 s (the sampling frequency was 10 Hz). The maximum linear speed and the maximum step

length of each robot were set to 0.3 m/s and 0.4 m, respectively.

In each experiment, the concentration threshold for the three robots to find the plume was set to 15 ppm. During the plume tracking, if the best global location of the three robots changed by less than or equal to 0.4 m (equal to one step) in 5 consecutive steps, the robots concluded that they had entered a local extremum area and then used the concentration maximization method to confirm whether they had reached the source. The concentration threshold for source declaration was set to 60 ppm. The other parameter settings of the proposed method are listed in Table 2.

Table 2. Parameter settings of the proposed source localization method

w	l_1	l_2	l_3	l_4	c_{\min}	c_{\max}	V_{\max}
1	2	2	0.5	0.5	15 ppm	60 ppm	0.4 m

To avoid spending too much time on a single experiment, if the robots had moved 50 steps (approximately 15 minutes), the robots terminated the source localization process. After the source localization process was terminated, if the distance between the source location determined by the robot (best global location) and the actual source location did not exceed 0.5 m, it was considered that the robots had successfully found the source; otherwise, the source localization experiment was considered to have failed. This localization error (0.5 m) is small enough to generally meet the requirements of practical applications [44]. In addition, robots can use a camera or other device to accurately determine the source location when the source is close enough [45, 46].

3.2 Setup of the numerical experiments

Based on the robot experiments in a real environment, we further conducted numerical simulations to validate whether the results obtained from numerical simulations are consistent with those obtained from real robot experiments. According to the real experimental environment, a CFD model was first built. Through CFD simulations, the airflow and ethanol concentration data were obtained. With these data, three simulated robots were used to locate the source on the MATLAB platform. Finally, the simulated results were compared with the experimental results.

To simplify the calculations in the CFD simulation, the circular fan was modeled as a square inlet and outlet ($0.3\text{ m} \times 0.3\text{ m}$) (Fig. 5). The air supply speed of the inlet was 1.6 m/s , the left and right swing period was 24 s , and the swing range was $0\text{--}100^\circ$. In addition, for simplification, no heat source was set in the CFD model, and the supply air temperature was set to $20\text{ }^\circ\text{C}$. Other settings (such as source location, release rate, obstacles, etc.) were identical to those in the experimental environment (Fig. 3). The simulation results of CFD are presented in Appendix A.

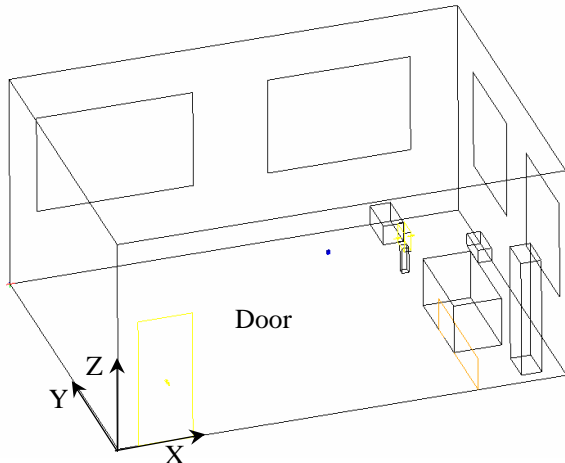


Fig. 5. CFD model of the experimental environment

For simplicity, the volume of each simulated robot was ignored in the source localization process on the MATLAB platform. However, like the real robots, each simulated robot also adopted the “move-stop-move” strategy, moving forward by one step for 10 s and then collecting concentrations for 5 s. Other settings during the simulated source localization process (such as each robot's maximum moving step length, the concentration threshold for plume finding and source declaration, the obstacle avoidance algorithm, etc.) were identical to those in the real robot experiments.

3.3 Numerical study of typical cases

After it had been validated that the results obtained from numerical simulations agreed well with those obtained from robot experiments, we further tested the proposed method in a simulated office ($X \times Y \times Z = 7.5 \text{ m} \times 2.7 \text{ m} \times 5.0 \text{ m}$) with two typical ventilation modes: mixing ventilation and natural ventilation. In the mixing

ventilation case, all the doors and windows were closed, and the air supply direction of each air supply inlet ($0.4 \text{ m} \times 0.3 \text{ m}$) changed periodically with time, but the air velocity remained unchanged; these conditions created a typical dynamic indoor environment with mechanical ventilation (Fig. 6). In the natural ventilation case, the east window ($0.4 \text{ m} \times 0.3 \text{ m}$) and east door ($0.75 \text{ m} \times 1.8 \text{ m}$) were opened to create a typical natural ventilation environment (Fig. 7). A potential ethanol source ($X \times Y \times Z=0.1 \text{ m} \times 0.1 \text{ m} \times 0.1 \text{ m}$) and four obstacles were built in each ventilation mode (Fig. 6 and 7). The release rate of ethanol was set to 12.5 mg/s in each numerical scenario, identical to that in the real robot experiments. For simplicity, each model in Fig. 2 had no heat source, and the air supplied in each model had a temperature of 20°C .

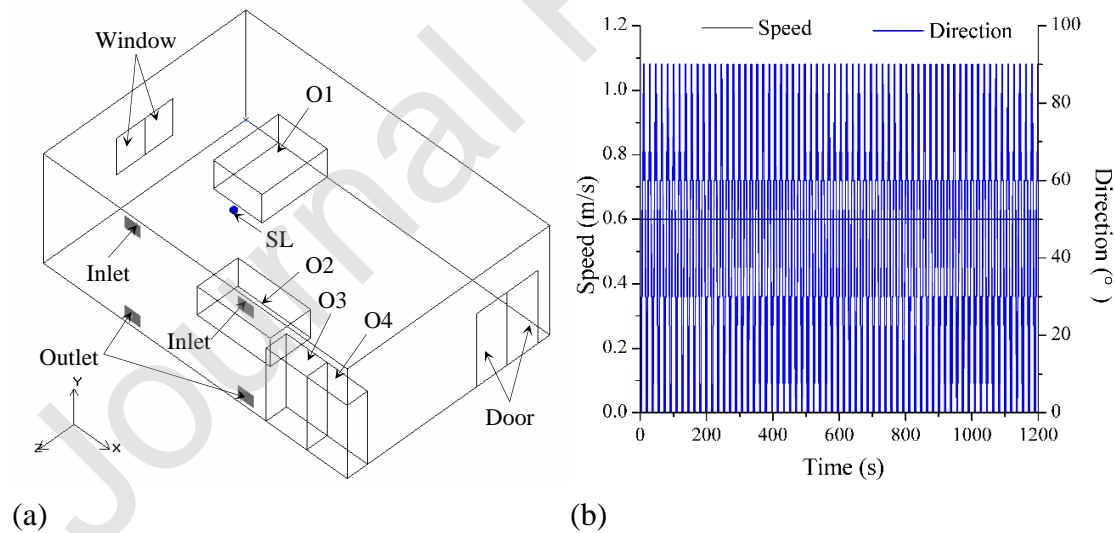


Fig. 6. Mixing ventilation office: (a) 3D model; (b) Air supply mode (SL: potential source location; O1–O4: obstacles)

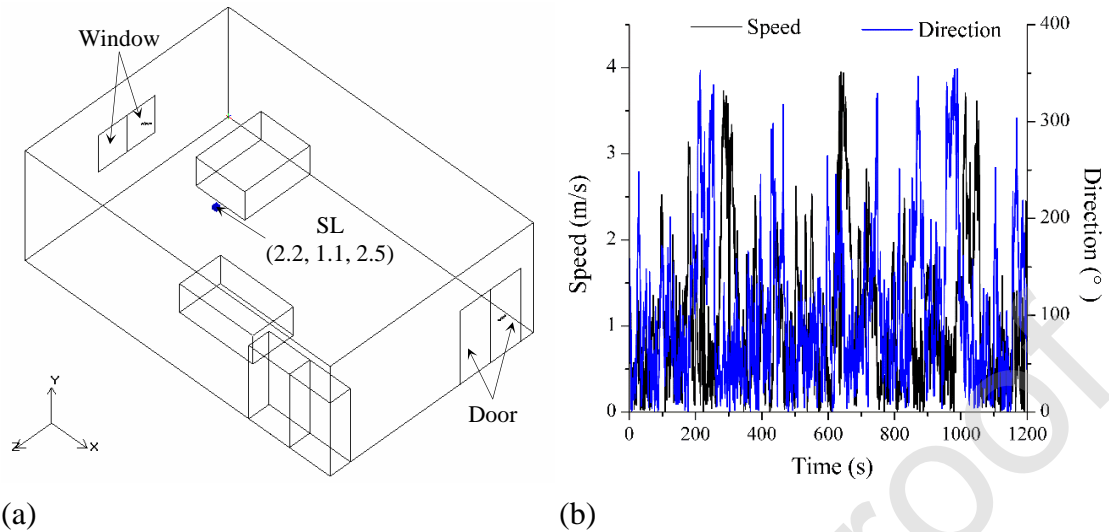


Fig. 7. Natural ventilation office: (a) 3D model; (b) Air supply mode

To further test the effectiveness of the multi-robot active olfaction method for different time-varying indoor airflow environments, we set two release scenarios in a simulated office ventilated by two typical air supply patterns, namely, MV (Fig. 6) and NV (Fig. 7). The method was numerically validated by the following two steps. First, the airflow fields and concentration distributions in each release scenario were simulated by CFD. Second, with the data obtained by CFD simulations, the source localization processes using the presented method were simulated on the MATLAB platform.

The dynamic airflow field and transient contaminant dispersion in each release scenario were simulated using the commercial CFD software Airpak (version 3.0). This software is widely applied and has been validated in indoor airflow and

contaminant dispersion studies [47]. The dynamic indoor airflow was simulated by an RNG k- ϵ model to achieve a balance between computational accuracy and time consumption [13]. To improve accuracy and ensure convergence, a Hexahedra element mesh was applied for discretization, and a second-order upwind scheme and linear underrelaxation iteration were used during the solution process. In each case, source release started after 300 s, and the contaminant dispersion process was simulated for 1200 s with a time step of 1 s. The simulation results are given in Appendix B.

In the two scenarios, six robots (R1–R6) started moving from the same locations (4.0 m, 0.1 m, and 2.0 m) on the floor after the contaminant had been released for 60 s (the room was ventilated for 360 s). The movement speeds of each robot in the vertical direction (Y axis) and in the horizontal plane (XZ plane) were 0.1 m/s and 0.3 m/s, respectively, and the horizontal projection angle between any two adjacent trajectories of the robots was 60°. Other settings during the simulated source localization process (such as each robot's maximum moving step length, the concentration threshold for plume finding and source declaration, the obstacle avoidance algorithm, etc.) were identical to those in the real robot experiments. In addition, we assumed that source localization was successful if the distance between the source location reported by the robots and the actual source location was within 0.5 m. For simplicity, ideal sensors without considering the response characteristics of real sensors were used in the simulated source localization process.

4. Results and discussion

4.1 Robot experiments

According to the experimental setup in Section 3.2, three mobile robots were used to conduct 15 independent source localization experiments. The source was successfully located in 12 experiments (only 3 experiments failed), and the success rate (the number of successful experiments divided by the number of total experiments) was 80%. These results show that the proposed method has strong robustness in dynamic indoor environments.

Fig. 8 shows the source localization process of the robots (R1–R3) and the maximum time-averaged concentration collected by the robots at each step in a typical successful experiment (the video of the experiment is provided in the supplemental material). After the robots departed, they experienced the stages of finding the plume, tracking the plume, trapping into a local extremum area, escaping from this area, rediscovering the plume and then tracking the plume again. During the tracking process, the robots continuously confirmed whether they had found the source. Finally, the robots successfully located the source at the 34th step.

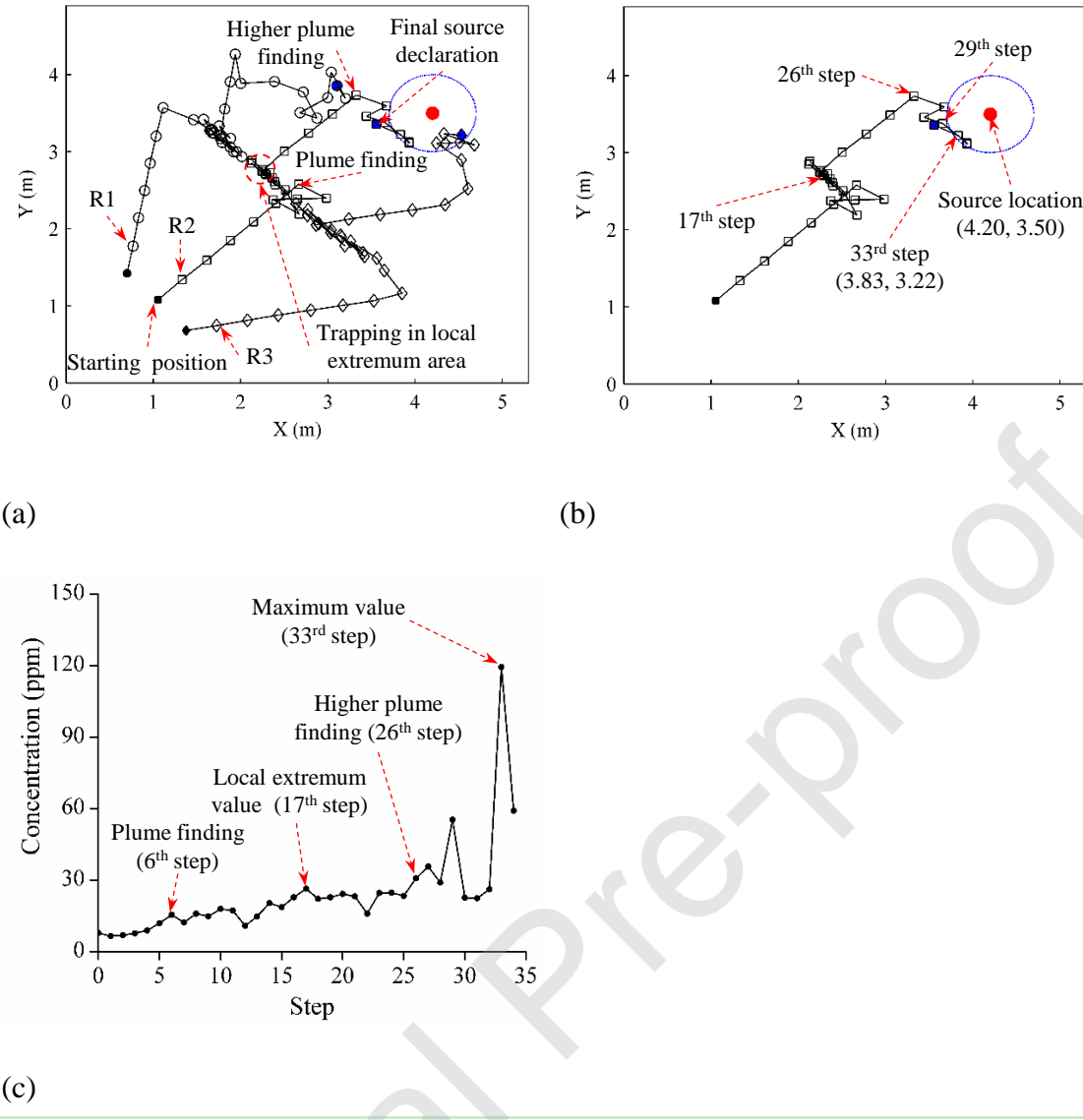


Fig. 8. A successful experiment: (a) trajectories of robots R1–R3; (b) trajectory of R2; (c) maximum time-averaged concentration collected by R1–R3 at each step

As shown in Fig. 8, the robots (R1–R3) first used a divergence search strategy to move straight in different directions to quickly find the plume. After R2 found the plume at the 6th step, all the robots switched to tracking the plume. At the 17th step, R2 detected a higher time-averaged concentration (26.42 ppm), which was less than

the threshold c_{\max} (60 ppm). In the next 5 consecutive steps, R1–R3 did not find a higher concentration; therefore, they determined that a local extremum area had been found according to the maximum concentration method. Subsequently, the robots used the divergence search strategy to quickly escape this area and try to find a higher concentration.

After the 26th step, R1–R3 escaped from the local extremum area and tracked the plume again. At the 29th step, R2 detected a higher time-averaged concentration and approached the vicinity of the source (Figs. 8(b) and 8(c)). At the 33rd step, R2 detected a higher concentration and reached the vicinity of the source (Figs. 8(b) and 8(c)). Subsequently, the robots determined that the source had been successfully located according to the maximum concentration method and ended the source localization process. The distance between the source location determined by the robots and the actual source location was 0.46 m (less than 0.5 m), indicating that this experiment was successful.

The results of one failed experiment for locating the source are shown in Fig. 9 (the video of the experiment is provided in the supplemental material). The robots experienced the stages of finding the plume, tracking the plume, two instances of trapping into and escaping from a local extremum area, rediscovering the plume and then tracking the plume again. Finally, after the 50th step, the robots still had not found the source and ended the source localization process. This source localization process was similar to that of Fig. 8. To make this paper more concise, we only briefly describe the source localization process and highlight the differences between Fig. 9

and Fig. 8.

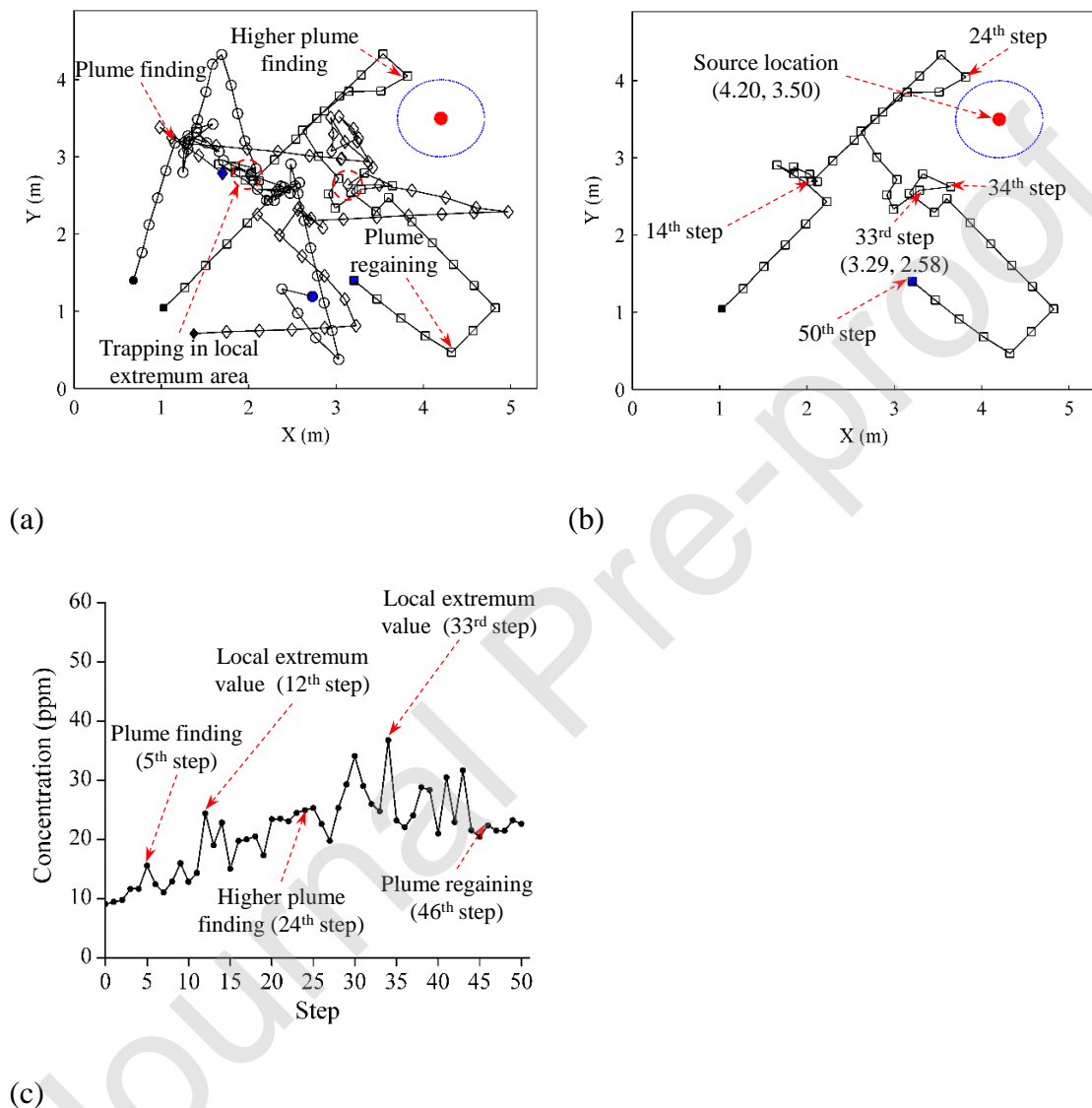


Fig. 9. A failed experiment: (a) trajectories of robots R1–R3; (b) trajectory of R2; (c) maximum time-averaged concentration collected by R1–R3 at each step

The robots (R1–R3) first moved straight in different directions until they found the plume at the 5th step. After finding the plume, R1–R3 tracked the plume and found a local extremum area at the 12th step. Subsequently, they moved straight in different directions to escape this area and rediscover the plume. At the 24th step, R2 detected a higher time-averaged concentration and escaped from the local extremum area. Subsequently, R1–R3 tracked the plume again and found a local extremum area at the 33rd step. Then, they repeated the above processes until the number of steps moved by each robot reached to the preset maximum steps (50 steps).

Further analysis of Fig. 9 reveals that robot R2 detected a higher concentration and approached the vicinity of the source at the 24th step, but it moved away from the source in the next step according to the improved PSO algorithm, which caused it to fail to detect a higher concentration again. The above results indicate that the improved PSO algorithm may lead the robots to move away from the source, making it more difficult to continuously track the plume. In addition, although robot R2 was closer to the source from the 33rd step to the 34th step, it failed to detect a higher concentration, which also caused it to move away from the source in the next step. These results indicate that, partly due to the periodic variation in the air supply direction of the fan, the airflow direction and contaminant concentration near the source fluctuated greatly with time, which may have also caused the robots to move away from the source and made it more difficult to continuously track the plume.

4.2 Numerical simulations of robot experiments

Table 3 summarizes the statistical results of the robot source localization experiments and simulated experiments. The success rate achieved by the numerical simulations was consistent with that obtained in experiments, and both were 80%; the average and standard deviation of the number of steps from numerical simulations were slightly smaller (6.5 steps and 2.3 steps, respectively) than those from robot experiments. These results indicate that the results obtained by numerical simulations agree well with those obtained by robot experiments and the numerical method can be used to test the effectiveness of the source localization method. In addition, one reason for the differences in the average and standard deviation of the number of steps is that the experimental conditions (such as source release time and rate, indoor temperature, airflow field, etc.) were difficult to maintain the same during each independent robot experiment, which may cause a larger difference in the number of steps required to locate the source in each experiment. The other reason is that in the real experiments, the gas sensors had detection errors and delays, which may increase the number of steps required to locate the source.

Table 3. Statistical results of robot experiments and simulated experiments for locating the source

Method	Success rate	Average number of steps	Standard deviation of the number of steps
Experiment	80% (12/15)	36.7	7.4
Simulation	80% (12/15)	30.2	5.1

4.3 Numerical case study

In the two scenarios, MV and NV, the robots could successfully locate the contaminant source. Fig. 10 shows the source locating process of the method in scenario NV, which represents a scenario with a dramatic change in the airflow field. After departing from the starting positions, the six robots first found the plume using the divergence search strategy after moving for 6 steps, then tracked the plume according to the improved PSO algorithm and were subsequently trapped in a local extremum area. After the robots confirmed that this area was distant from the source by using the maximum concentration method, they used the divergence search strategy to escape from this area. The robots then repeated the above processes until they found the source. From departure to successfully locating the source, the overall localization time was 29 steps.

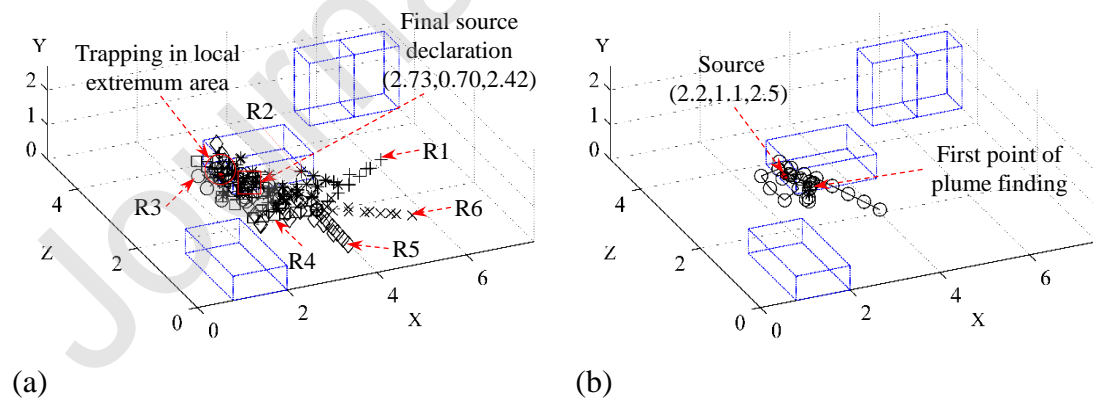


Fig. 10. The process of source localization using the improved method in an office with NV: (a) trajectories of R1–R6; (b) trajectory of R3

To improve the credibility of the statistical results of numerical experiments, we first conducted 200 independent experiments using the proposed method for each release scenario (MV and NV) and then randomly divided these 200 experiments into two independent groups (A1 and A2; B1 and B2) for each release scenario for statistical analysis (Table 4). As shown in Table 4, the number of successful experiments from groups A1, A2, B1 and B2 were 92, 92, 76 and 76, respectively, indicating that the success rate achieved in each independent group for each release scenario did not differ. To further analyze whether the difference between the two independent groups for each release scenario was significant, Student's t-test was used, and two null assumptions were made as follows: $H_0: \mu_{A1} = \mu_{A2}$; $H_0': \mu_{B1} = \mu_{B2}$. According to the principle of Student's t-test [48], the t -values calculated for each release scenario were 0.4162 and 0.4904, with 182 and 150 degrees of freedom, respectively. Because the t -values for each release scenario were much less than $t_{0.05} n \approx 1.960$ ($n \geq 100$), the p -values for MV and NV were 0.7338 and 0.6245 (much higher than 0.05), respectively, indicating that the differences between the two independent groups for MV and NV were not significant. These results of Student's t-tests for MV and NV fully indicate that 100 independent experiments are sufficient for statistical analysis of the proposed method for each release scenario.

Table 4. Statistical tests using the proposed method to locate the source in two simulated release scenarios

Release scenario	Group number	Successful experiments/Total number of experiments	Average number of steps	Standard deviation of the number of steps
MV	A1	92/100	24.2	3.4
	A2	92/100	24.0	3.1
NV	B1	76/100	29.9	6.5
	B2	76/100	29.4	6.0

Further analysis of Table 4 shows that the success rate achieved by the proposed method in MV was 16% higher than that in NV; the average and standard deviation of the number of steps in NV were approximately 0.2 times and 1 time higher than those in MV, respectively. The main reason for the above differences is that compared to the MV scenario, the fluctuations in airflow and contaminant concentration in the NV scenario are more irregular, and the amplitudes of these fluctuations are larger (Appendix B). The above results indicate that irregular and large fluctuations in airflow and concentration in a dynamic indoor environment can make it more difficult for robots to locate the source and further decrease the success rate and efficiency of source localization.

4.4 Method comparison

For comparison, the statistical results of independent experiments using the standard PSO-based method (SPSO), wind utilization II (WUII) and the improved method (IPSO) are listed in Table 5. In the two typical release scenarios, MV and NV,

the success rates achieved by the IPSO method (92% and 76%, respectively) were much higher than those achieved by the SPSO method (64% and 65%, respectively) and WUII method (53% and 62%, respectively), indicating that the improved method can achieve a higher success rate in dynamic airflow environments than the comparison methods. The main reason for the above differences is that compared to the SPSO and WUII methods, the IPSO method can enhance the search capability by introducing extremum disturbance factors to prevent the robots from becoming trapped into a local optimum and guide the robots to move toward an area with higher concentration.

From the perspective of source localization efficiency, the average number of steps moved under the IPSO method, SPSO method and WUII method was similar in each release scenario. For MV and NV, the maximum average number of steps of the three methods was only 2.4 steps and 3.9 steps greater than the minimum average number of steps, respectively.

Table 5. Performance of the SPSO, WUII and IPSO methods for source localization in two typical release scenarios*

Release scenario	Success rate			Average number of steps			Standard deviation of the number of steps		
	SPSO	WUII	IPSO	SPSO	WUII	IPSO	SPSO	WUII	IPSO
MV	64%	53%	92%	21.8	22.6	24.2	2.3	3.0	3.4
NV	65%	62%	76%	33.8	32.6	29.9	7.2	7.9	6.5

* In each scenario, 100 independent experiments were conducted.

4.5. Limitations and future study

This work assumed that the contaminant was released from only one source in each scenario. This assumption excludes the application of the method in some situations where multiple sources release contaminants simultaneously or sequentially. Nevertheless, a variety of leakage scenarios satisfy this assumption in practice, such as hazardous gas release from the orifice of a gas pipeline or container.

This study also assumed that the release rate of the contaminant source remains constant in each scenario. In this study, we focused on investigating the effect of dynamic indoor airflows on source localization and only considered a constant source due to the word limit. In the future, we will further study the localization of time-varying contaminant sources and analyze the effect of time-varying contaminant sources on the source localization method under dynamic airflow.

The concentration threshold for source declaration should also be known in advance. In this study, this threshold was obtained by collecting concentrations at 8 points equally spaced on a circle centered on the source and having a radius of 0.5 m before the experiments and then calculating the average of the concentrations. For practical applications, we recommend that before the robots are put into use, a certain number of robot experiments or numerical experiments should be conducted to determine a reasonable concentration threshold.

Considering the word limit, this study focused on experimentally and numerically testing the source localization method from a dynamic airflow perspective. In the

future, we will further study how to optimize this method from the perspectives of the method parameters (e.g., the dimensionless parameters w , l_1 and l_2 in Eq. (4) and the concentration threshold for source declaration), the robots (e.g., the number of robots used and their starting positions) and the sensors (sensor threshold and detection error).

5. Conclusions

To solve the challenging source localization problem in dynamic indoor environments, this paper presented a multi-robot olfaction method (IPSO) independent of airflow information. The method includes three core algorithms: the improved PSO algorithm for plume tracking, the maximum concentration method for source declaration and the divergence search strategy for plume finding and escaping from a local extremum area. To avoid being trapped in local extremum areas, the improved PSO algorithm maintains the diversity of the robots and enlarges their search scope by introducing extremum disturbance factors into the standard PSO algorithm. The effectiveness of the presented method was validated by combining robot experiments with numerical simulations. The performance of the presented method was further compared with that of two other PSO-based source localization methods (SPSO and WUII) by numerical experiments. Through robot experiments and numerical simulations, we can draw the following conclusions:

- (1) The proposed method can help robots successfully escape local extremum areas and rapidly find the contaminant source in dynamic indoor environments.

- (2) In an experimental environment with a fan swinging from left to right, the proposed method proved robust in locating the contaminant source, with a success rate of 80%.
- (3) The IPSO method was further compared with the SPSO and WUII methods in mixing ventilation (MV) and natural ventilation (NV) cases by numerical experiments. In the MV case, the IPSO, SPSO and WUII methods achieved success rates of 92%, 64% and 53% and averages of 21.8, 22.6 and 24.2 steps, respectively; in the NV case, the IPSO, SPSO and WUII methods achieved success rates of 76%, 65% and 62% and averages of 33.8, 32.6 and 29.9 steps, respectively. These results show that in dynamic indoor environments with mechanical and natural ventilation, the success rates of the presented method were higher than those of the SPSO and WUII methods and that the average numbers of steps of the three methods were close.

Acknowledgments

This study was supported by the National Natural Science Foundation of China (Grant No. 51478468) and the National Program on Key Basic Research Project (973 Program, Grant No. 2015CB058003). This study was also supported by the National Natural Science Foundation of China (Grant No. 51708286), the China National Key R&D Program (Grant No. 2018YFC0705201), and the Natural Science Foundation of Jiangsu Province (Grant No. BK20171015).

Appendix A. Simulated airflow field and contaminant dispersion in the robot experimental environment

Fig. A.1 shows the simulated airflow field in the robot experimental environment.

Air was blown by the fan toward the opposite wall, then flowed along the opposite sidewall to the southwest door and created a large vortex on the south side of the laboratory.

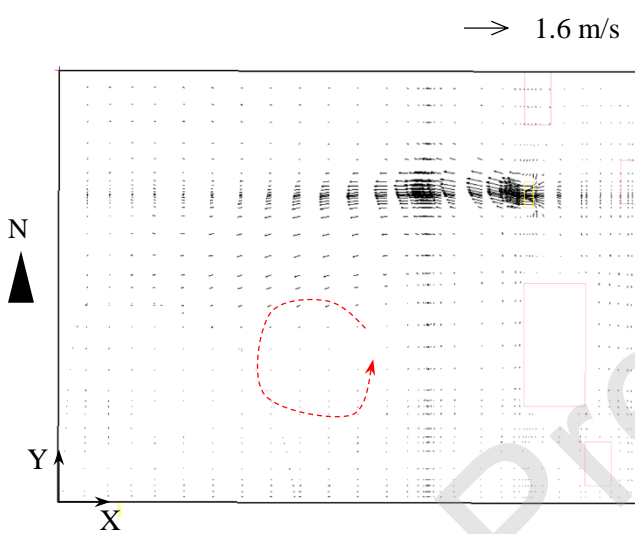


Fig. A.1. Simulated airflow field in the XY plane ($Z=0.55$ m) of the laboratory through the center point of the source after fan operation for 500 s

Fig. A.2 shows that the air speed and direction at the center point of the source varied with time periodically, indicating that the airflow at the source location was affected by the swinging of the fan from left to right.

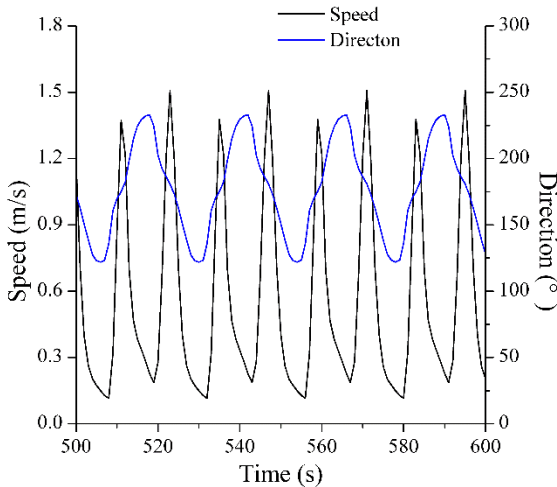


Fig. A.2. Simulated air speed and direction at the center point of the source in the robot experimental environment

Fig. A.3 shows the concentration distribution of ethanol at different time points after the ethanol vapor was released. The concentration distribution swung with the airflow, and an obvious extremum area was generated around the source.

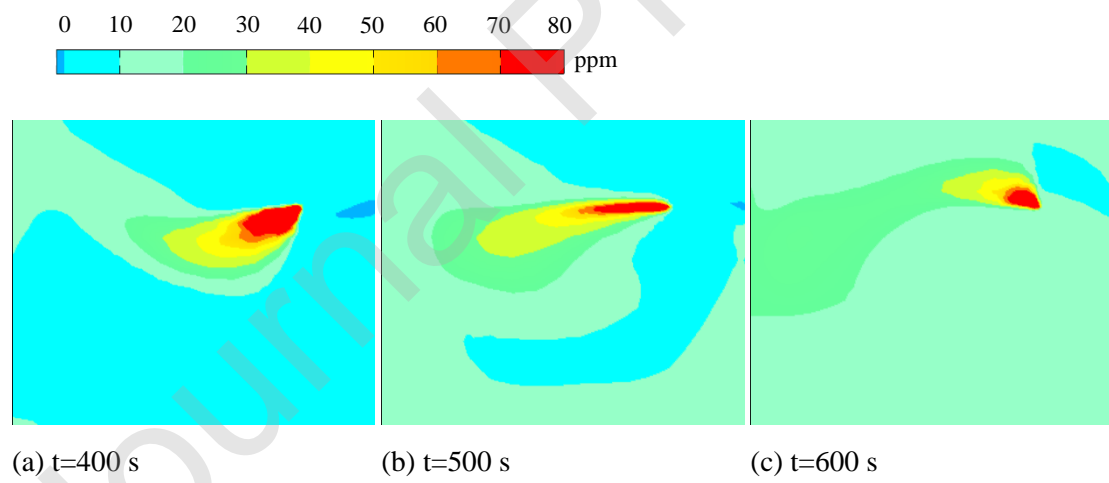


Fig. A.3. Simulated concentration distributions of ethanol in the YZ plane ($X=2.2\text{ m}$) in the robot experimental environment

Appendix B. Simulated airflow field and contaminant dispersion in the case study

Fig. A.4 shows the airflow fields in the two typical ventilation cases, MV and NV.

In MV, air was supplied into the room through two inlets in the opposite sidewall, flowed along the sidewall to the floor, and was finally exhausted through two outlets. Since the air supply swung periodically from up to down, the airflow in the YZ plane was uniformly distributed, and no obvious vortex was generated. In NV, fresh air was supplied from the open window, flowed to the opposite sidewall and finally vented through the open door. Due to the disordered supply of fresh air through the window, the airflow distribution was chaotic, and several vortexes were generated.

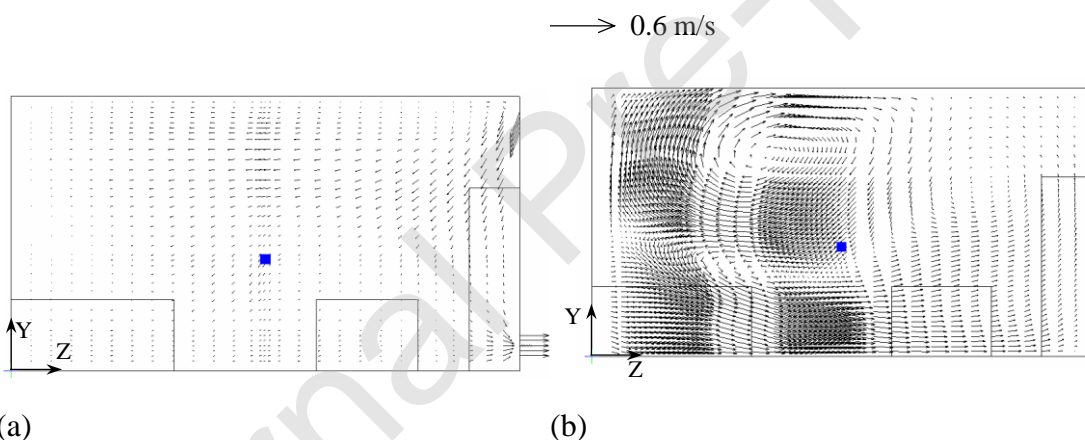


Fig. A.4. Simulated airflow field in the YZ plane ($X=2.2$ m) through the center point of the source at 500 s after the office was ventilated with different air supply patterns:
(a) MV; (b) NV

Fig. A.5 shows that the airflow at the center point of the source varied with time in MV and NV. The air speed and direction showed great differences between the two

cases. In MV, the air speed and direction fluctuated periodically, and the magnitude of these fluctuations was small, while the air speed and direction varied substantially and randomly with time in NV. The large variations in air speed and direction signify that the concentration field in the office changes greatly, increasing the difficulty of source localization by the robots.

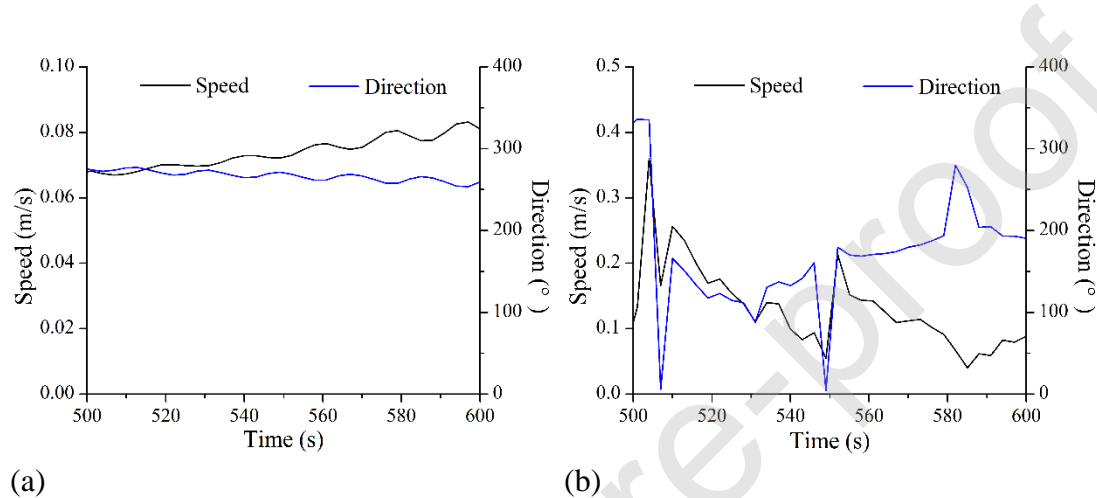


Fig. A.5. Simulated air speeds and directions at the center point of the source in each case with different air supply patterns: (a) MV; (b) NV

Fig. A.6 shows the contaminant distributions in MV and NV at different times after the contaminant was released. The contaminant distribution in each airflow field clearly differed. The contaminant extremum area around the release source was approximately elliptical in the airflow field of MV, while the extremum area was irregular and small in the airflow field of NV. In addition, the size of the extremum area decreased with time in the airflow field of MV but varied randomly with time in the airflow field of NV.

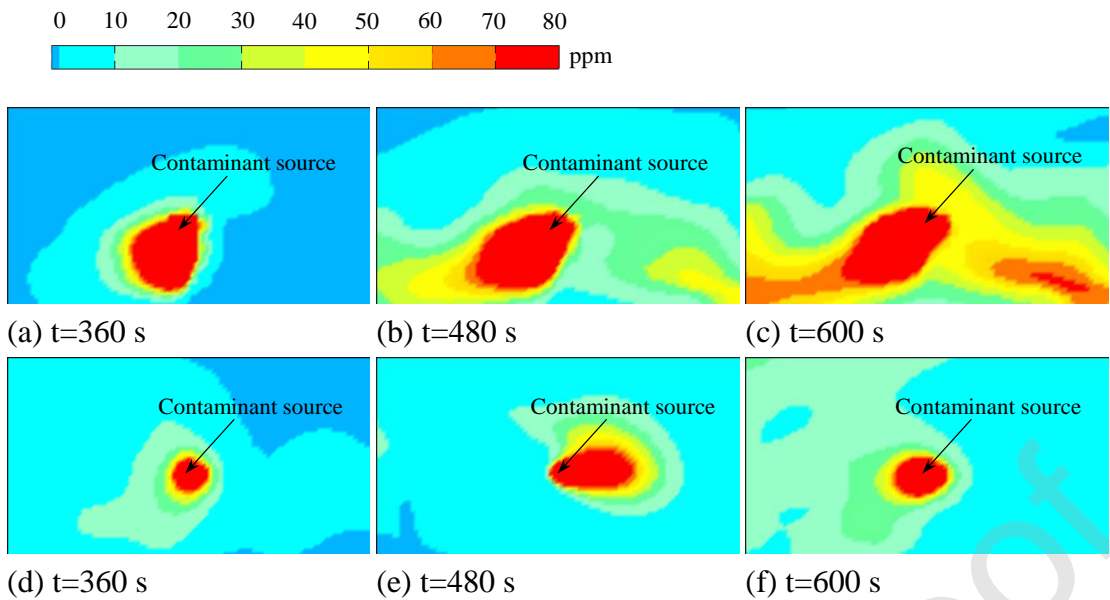


Fig. A.6. Simulated contaminant distributions in the YZ plane ($X=2.2$ m) in an office with different air supply patterns: (a)–(c) MV; (d)–(f) NV

References

- [1] M. Jin, S. Liu, S. Schiavon, C. Spanos, Automated mobile sensing: Towards high-granularity agile indoor environmental quality monitoring, *Build. Environ.* 127 (2018) 268–276.
- [2] M. Malayeri, F. Haghight, C.-S. Lee, Modeling of volatile organic compounds degradation by photocatalytic oxidation reactor in indoor air: A review, *Build. Environ.* (2019), doi: <https://doi.org/10.1016/j.buildenv.2019.02.023>.
- [3] X.F. Shan, W. Xu, Y.K. Lee, W.Z. Lu, Evaluation of thermal environment by coupling CFD analysis and wireless-sensor measurements of a full-scale room with cooling system, *Sust. Cities Soc.* 45 (2019) 395–405.
- [4] Z.J. Liu, S.Y. Ma, G.Q. Cao, C. Meng, B.J. He, Distribution characteristics, growth, reproduction and transmission modes and control strategies for microbial contamination in HVAC systems: A literature review, *Energy Build.* 177 (2018) 77–95.
- [5] H. Cai, X.T. Li, Z.L. Chen, M.Y. Wang, Rapid identification of multiple constantly-released contaminant sources in indoor environments with unknown release time, *Build. Environ.* 81 (2014) 7–19.
- [6] X. Liu, Z. Zhai, Inverse modeling methods for indoor airborne pollutant tracking: literature review and fundamentals, *Indoor Air* 17 (6) (2007) 419–38.
- [7] G.L. Liu, M.X. Xiao, X.X. Zhang, C. Gal, X.J. Chen, L. Liu, S. Pan, J.S. Wu, L. Tang, D. Clements-Croome, A review of air filtration technologies for sustainable and healthy building ventilation, *Sust. Cities Soc.* 32 (2017) 375–396.

- [8] N.R. Martins, G.C. da Graca, Impact of PM2.5 in indoor urban environments: A review, *Sust. Cities Soc.* 42 (2018) 259–275.
- [9] Z.Q. Zhai, X. Liu, H.D. Wang, Y.G. Li, J.J. Liu, Experimental verification of tracking algorithm for dynamically-releasing single indoor contaminant, *Build. Simul.* 5 (1) (2012) 5–14.
- [10] X. Liu, Z.Q.J. Zhai, Prompt tracking of indoor airborne contaminant source location with probability-based inverse multi-zone modeling, *Build. Environ.* 44 (6) (2009) 1135–1143.
- [11] Y.C. Chen, H. Cai, Z.L. Chen, Q.L. Feng, Using multi-robot active olfaction method to locate time-varying contaminant source in indoor environment, *Build. Environ.* 118 (2017) 101–112.
- [12] B. Wang, A. Malkawi, Design-based natural ventilation evaluation in early stage for high performance buildings, *Sust. Cities Soc.* 45 (2019) 25–37.
- [13] H.D. Wang, S. Lu, J.J. Cheng, Z.Q. Zhai, Inverse modeling of indoor instantaneous airborne contaminant source location with adjoint probability-based method under dynamic airflow field, *Build. Environ.* 117 (2017) 178–190.
- [14] M. Hutchinson, H. Oh, W.H. Chen, A review of source term estimation methods for atmospheric dispersion events using static or mobile sensors, *Inform. Fusion* 36 (2017) 130–138.
- [15] G. Biros, O. Ghattas, K.R. Long, B.V.B. Waanders, A variational finite element method for source inversion for convective-diffusive transport, *Finite Elem. Anal. Des.* 39 (8) (2003) 683–705.

- [16] M.D. Sohn, R.G. Sextro, A.J. Gadgil, J.M. Daisey, Responding to sudden pollutant release in office buildings: 1. Framework and analysis tools, *Indoor Air* 13 (3) (2003) 267–276.
- [17] P. Sreedharan, M.D. Sohn, W.W. Nazaroff, A.J. Gadgil, Influence of indoor transport and mixing time scales on the performance of sensor systems for characterizing contaminant releases, *Atmos. Environ.* 41 (40) (2007) 9530–9542.
- [18] T. Zhang, Q. Chen, Identification of contaminant sources in enclosed environments by inverse CFD modeling, *Indoor Air* 17 (3) (2007) 167–177.
- [19] X. Liu, Z. Zhai, Location identification for indoor instantaneous point contaminant source by probability-based inverse Computational Fluid Dynamics modeling, *Indoor Air* 18 (1) (2008) 2–11.
- [20] A. Bastani, F. Haghishat, J.A. Kozinski, Contaminant source identification within a building: Toward design of immune buildings, *Build. Environ.* 51(5) (2012) 320–329.
- [21] H. Cai, X.T. Li, Z.L. Chen, L.J. Kong, Fast identification of multiple indoor constant contaminant sources by ideal sensors: A theoretical model and numerical validation, *Indoor Built Environ.* 22 (6) (2013) 897–909.
- [22] P.M. Tagade, B.M. Jeong, H.L. Choi, A Gaussian process emulator approach for rapid contaminant characterization with an integrated multizone-CFD model, *Build. Environ.* 70 (2013) 232–244.
- [23] X.L. Shao, X.T. Li, H.Y. Ma, Identification of constant contaminant sources in a test chamber with real sensors, *Indoor Built Environ.* 25 (6) (2016) 997–1010.

- [24] Y. Xue, Z.Q. Zhai, Inverse identification of multiple outdoor pollutant sources with a mobile sensor, *Build. Simul.* 10 (2) (2017) 255–263.
- [25] A.J. Lilienthal, A. Loutfi, T. Duckett, Airborne chemical sensing with mobile robots, *Sensors* 6 (11) (2006) 1616–1678.
- [26] H. Ishida, Y. Wada, H. Matsukura, Chemical sensing in robotic applications: A review, *IEEE Sens. J.* 12 (11) (2012) 3163–3173.
- [27] X.-x. Chen, J. Huang, Odor source localization algorithms on mobile robots: A review and future outlook, *Robot. Auton. Syst.* 112 (2019) 123–136.
- [28] A.T. Hayes, A. Martinoli, R.M. Goodman, Distributed odor source localization, *IEEE Sens. J.* 2 (3) (2002) 260–271.
- [29] H. Ishida, Y. Kagawa, T. Nakamoto, T. Moriizumi, Odor-source localization in the clean room by an autonomous mobile sensing system, *Sensor. Actuat. B-Chem.* 33 (1–3) (1996) 115–121.
- [30] A. Lilienthal, T. Duckett, Experimental analysis of gas-sensitive Braitenberg vehicles, *Adv. Robotics* 18 (8) (2004) 817–834.
- [31] A. Marjovi, L. Marques, Multi-robot olfactory search in structured environments, *Robot. Auton. Syst.* 59 (11) (2011) 867–881.
- [32] M. Awadalla, T.F. Lu, Z.F. Tian, B. Dally, Z.Z. Liu, 3D framework combining CFD and MATLAB techniques for plume source localization research, *Build. Environ.* 70 (2013) 10–19.
- [33] A. Marjovi, L. Marques, Optimal spatial formation of swarm robotic gas sensors in odor plume finding, *Auton. Robot.* 35 (2–3) (2013) 93–109.

- [34] Q. Feng, H. Cai, F. Li, Y. Yang, Z. Chen, Locating time-varying contaminant sources in 3D indoor environments with three typical ventilation systems using a multi-robot active olfaction method, *Build. Simul.* 11 (3) (2018) 597–611.
- [35] Q. Feng, H. Cai, F. Li, X. Liu, S. Liu, J. Xu, An improved particle swarm optimization method for locating time-varying indoor particle sources, *Build. Environ.* 147 (2019) 146–157.
- [36] D.H. Luo, Multi-robot odor source localization strategy based on a modified ant colony algorithm, *Robot* 30 (6) (2008) 536–541.
- [37] Q.H. Meng, W.X. Yang, Y. Wang, F. Li, M. Zeng, Adapting an ant colony metaphor for multi-robot chemical plume tracing, *Sensors* 12 (4) (2012) 4737–4763.
- [38] W. Jatmiko, K. Sekiyama, T. Fukuda, A PSO-based mobile robot for odor source localization in dynamic advection-diffusion with obstacles environment: Theory, simulation and measurement, *IEEE Comput. Intell. M.* 2(2) (2007) 37–51.
- [39] L. Marques, U. Nunes, A.T. de Almeida, Particle swarm-based olfactory guided search, *Auton. Robot.* 20 (3) (2006) 277–287.
- [40] D.W. Gong, Y. Zhang, C.L. Qi, Localising odour source using multi-robot and anemotaxis-based particle swarm optimisation, *Iet Control Theory A.* 6 (11) (2012) 1661–1670.
- [41] Y.T. Yan, R. Zhang, J. Wang, J.M. Li, Modified PSO algorithms with "Request and Reset" for leak source localization using multiple robots, *Neurocomputing* 292 (2018) 82–90.
- [42] J. Burgues, V. Hernandez, A.J. Lilienthal, S. Marco, Smelling nano aerial vehicle

for gas source localization and mapping, Sensors 19 (3) (2019).

[43] K. Kamarudin, A.Y.M. Shakaff, V.H. Bennetts, S.M. Mamduh, A. Zakaria, R. Visvanathan, A.S.A. Yeon, L.M. Kamarudin, Integrating SLAM and gas distribution mapping (SLAM-GDM) for real-time gas source localization, Adv. Robotics 32 (17) (2018) 903–917.

[44] J.G. Li, Q.H. Meng, Y. Wang, M. Zeng, Odor source localization using a mobile robot in outdoor airflow environments with a particle filter algorithm, Auton. Robot. 30 (3) (2011) 281–292.

[45] H. Ishida, H. Tanaka, H. Taniguchi, T. Moriizumi, Mobile robot navigation using vision and olfaction to search for a gas/odor source, Auton. Robot. 20 (3) (2006) 231–238.

[46] J. Monroy, J.R. Ruiz-Sarmiento, F.A. Moreno, F. Melendez-Fernandez, C. Galindo, J. Gonzalez-Jimenez, A semantic-based gas source localization with a mobile robot combining vision and chemical sensing, Sensors 18 (12) (2018) 4174.

[47] L. Xu, Effectiveness of hybrid air conditioning system in a residential house, Waseda University, Tokyo, Japan, 2003.

[48] M.H. DeGroot, M.J. Schervish, Probability and statistics (fourth edition), Pearson Education, 2012.